

Emergence of Unconventional Interfacial Spin Texture in Topological Insulator-Based Magnetic Heterostructures

Dhaval Suri,^{1,*} Archit Bhardwaj,¹ Satyaki Sasmal,¹ and Karthik V. Raman^{1,†}

¹*Tata Institute of Fundamental Research, Hyderabad, Telangana 500046, India*

In a topological insulator (TI)/magnetic insulator (MI) hetero-structure, large spin-orbit coupling of the TI and inversion symmetry breaking at the interface could foster non-planar spin textures such as skyrmions at the interface. This is observed as topological Hall effect in a conventional Hall set-up. While this effect has been observed at the interface of TI/MI, where MI beholds perpendicular magnetic anisotropy, non-trivial spin-textures that develop in interfacial MI with in-plane magnetic anisotropy is under-reported. In this work, we study Bi₂Te₃/EuS hetero-structure using planar Hall effect (PHE). We observe planar topological Hall and spontaneous planar Hall features that are characteristic of non-trivial in-plane spin textures at the interface. We find that the latter is minimum when the current and magnetic field directions are aligned parallel, and maximum when they are aligned perpendicularly within the sample plane, which maybe attributed to the underlying planar anisotropy of the spin-texture. These results demonstrate the importance of PHE for sensitive detection and characterization of non-trivial magnetic phase that has evaded exploration in the TI/MI interface.

Spin textures with non-trivial topology, also known as skyrmions are commonly observed in materials where non-centrosymmetry of the crystal leads to an unconventional exchange arising from the Dzyaloshinskii-Moriya (DM) interaction [1, 2]. Such spin textures can also be stabilized in proximity coupled hetero-structures of heavy metal (HM) and ferromagnet, by virtue of large spin-orbit coupling (SOC) of the HM and inversion symmetry breaking at the interface [3]. Topological insulators (TIs) offer yet another robust platform in this regard, whose high SOC is proven to give rise to skyrmions in proximitized ferromagnetic metals and insulators [4–10]. However, in comparison with ferromagnetic metals, manipulation of skyrmions in magnetic insulators (MI) provide a technological advantage due to the lower dissipative losses. Hence, the recent report of skyrmions appearing at the interface between an MI and a TI marks a significant progress [10]. Furthermore, investigating these TI/MI interfaces is fundamentally crucial to understand the interplay between the real-space topology of spin-textures and the band topology of TI [11].

The TI/MI interface has been extensively investigated for promising emergent quantum states [12–20] that arise by virtue of time reversal symmetry breaking of the TI surface states. However, the perspective of inverse proximity effect (IPE) whereby the large SOC of the TI affecting the magnetic properties of MI at the interface has received limited attention. Here we present the development of non-trivial spin-textures in EuS – an MI, interfaced with the Bi₂Te₃, a three dimensional TI. EuS is a Heisenberg ferromagnetic insulator with a Curie temperature of 16.6 K. In contrast to the experiment by Li et. al. [10], that used an MI with perpendicular magnetic anisotropy (PMA), we study EuS which has an in-plane anisotropy [21]. Studies of TI/EuS have shown strong enhancement in the Curie temperature of interfacial EuS with a weak out-of-plane anisotropy [17], which

was later found to be influenced by carrier mediated Ruderman–Kittel–Kasuya–Yosida interactions [19, 22]. Theoretically, formation of skyrmion states in such in-plane anisotropy materials emerge due to the development of weak out-of-plane anisotropy [23, 24]. Although spin canting of EuS moments at the interface was observed in these studies, the nature of spin texture remains an open question. In the present work we study TI/EuS electronically, and find signatures of non-trivial spin textures at the interface of TI/MI. Interestingly, by virtue of the compensating spin textures that develops in this interface [23, 25, 26], their electronic signature was not apparent in conventional Hall measurements, requiring a planar Hall measurement configuration to unveil its presence.

Planar Hall effect (PHE) refers to the development of a transverse voltage in response to longitudinal current and an in-plane magnetic field B , such that the influence of Lorentz force is absent [27, 28]. In a conventional ferromagnet or a TI, PHE depends on φ , the in-plane angle between current and magnetic field, as $R_{xy} \propto \sin 2\varphi$ and $R_{xx} \propto \cos^2 \varphi$, where R_{xy} is the planar Hall resistance (PHR) [10, 29] and R_{xx} is the planar magneto-resistance (PMR) [30]. As a result, the R_{xx} and R_{xy} signal are $\pi/4$ out-of-phase in φ . In addition, since the Lorentz force is absent in this configuration, the R_{xx} and R_{xy} signals are purely symmetric with respect to B . Therefore, any deviation from the above is often indicative of additional mechanisms that drive the unconventional PHE transport. In our study on Bi₂Te₃/EuS interface, we provide a comprehensive picture of such unconventional responses appearing in the PHR and PMR signals at low magnetic fields and associate them to the development of non-trivial spin textures in the EuS.

In this work, epitaxial films of Bi₂Te₃ (14 quintuple layers) are grown on Al₂O₃ (0001) substrate, followed by EuS (5 nm)/AlO_x ($x \sim 1.5 - 2$), using molecular beam

epitaxy technique (refer SI for details). The surface-state effect of TI is turned off by optimising the growth conditions such that the Fermi level is placed deep inside the conduction band. For the PHE studies, the as-grown films are patterned into a Hall bar device of channel length and width ≈ 3 mm and ≈ 1.5 mm respectively, by mechanical scratching to eliminate any possible contamination due to lithographic processes.

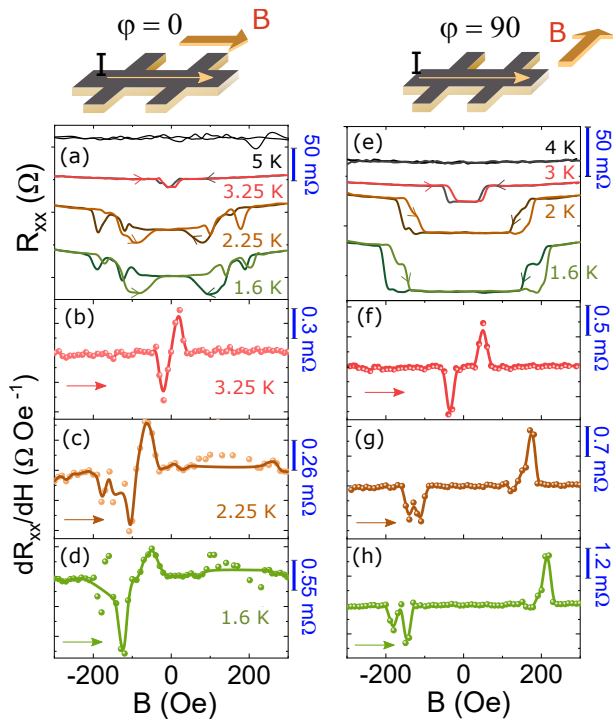


FIG. 1. PMR (R_{xx}) versus in-plane magnetic field (scan direction shown by arrows) at different temperatures, in the configuration (a) $\varphi = 0^\circ$ (e) $\varphi = 90^\circ$. The corresponding first derivatives of only the forward scans, in the configurations (b), (c) and (d) $\varphi = 0^\circ$ (f), (g) and (h) $\varphi = 90^\circ$.

In fig. 1, we investigate the PMR of the patterned device in low magnetic fields ($|B| < 300$ Oe) within the coercive field of the sample. The alignment of film-plane parallel to magnetic field is carefully performed by monitoring the minimum of the Hall voltage with varying out-of-plane angle θ (refer to SI). Fig. 1 (a) and (e) shows R_{xx} vs B , as a function of temperature (T) in the $\varphi = 0^\circ$ and $\varphi = 90^\circ$ configuration respectively, where φ is the angle between current and in-plane magnetic field. We find that R_{xx} is nearly independent of magnetic field down to 5 K. However, for $T < 4$ K, a step-like feature develops at low fields with the emergence of two hysteresis loops symmetric about $B = 0$. The origin of this hysteresis is different from the conventional hysteresis of a ferromagnet. In a ferromagnet, the resistance change occurs close to the film's coercive field upon reversing the direction of B . However in these devices, the transitions are observed much before the field reversal.

Hence, the observed unconventional step-like response in PMR indicates an emergent magnetic phase transition as seen by the derivative curves in fig. 1 (b)-(d) and (f)-(h) (shown only for the forward scans). On lowering the temperature, the magnetic field corresponding to these phase transition increases, implying higher stability of the emergent magnetic phase. Similar phase transitions have been commonly observed in systems such as MnSi that hosts skyrmionic spin textures [16, 25, 30–32]; this hints to the possible emergence of robust non-trivial spin textures at the $\text{Bi}_2\text{Te}_3/\text{EuS}$ interface in our devices. Magnetometry studies on these films (see SI) reveal that these transitions appear in the non-saturating state of EuS when the competing effects of internal exchange and anisotropy fields form a stable magnetic phase. Together with the inversion symmetry breaking and the large SOC of Bi_2Te_3 at the $\text{Bi}_2\text{Te}_3/\text{EuS}$ interface, conditions become conducive to generate strong interfacial DM interactions favoring the formation of non-trivial spin-textures. Interestingly, the PMR curves in $\varphi = 0^\circ$ and $\varphi = 90^\circ$ configuration exhibit contrasting responses with the latter configuration showing a larger region of plateau at low field and a relatively sharper transition as interpreted from the first derivative plots. All these observations suggest an in-plane anisotropy in probing these spin-textures.

Further, we analyse the PHR signal (R_{xy}) which was measured simultaneously with R_{xx} for the above two measurement configurations of φ . Fig. 2 (a) and (c) show R_{xy} vs B measured at different temperatures in $\varphi = 0^\circ$ and $\varphi = 90^\circ$ configurations, respectively. We notice a similar step-like profile at low fields below 4 K with the same form of anisotropy and hysteresis as in the R_{xx} signal, however predominantly with an inverted signal i.e., a drop in R_{xx} corresponds to a rise in R_{xy} . To characterize the magnetic phase formed at the $\text{Bi}_2\text{Te}_3/\text{EuS}$ interface, we analyse the emergence of hysteresis in R_{xy} by performing an elementary subtraction of the forward and backward scans (ΔR_{xy}) in fig. 2 (b) and (d). At 1.6 K, ΔR_{xy} peaks at ≈ 80 Oe and ≈ 160 Oe in the $\varphi = 0^\circ$ and $\varphi = 90^\circ$ configurations, respectively. Here, the sign reversal and the broadening of the hysteresis zone with cool down indicate the enhanced stabilization of the particular magnetic phase [33]. Similar responses in PHR accompanied by a hysteresis has been reported in studies of MnSi and FeGe [29, 30] and attributed to the formation of topologically conserved spin-textures such as skyrmions.

To examine the formation of spin-textures at the $\text{Bi}_2\text{Te}_3/\text{EuS}$ interface using PHE studies by decomposing the PHR and PMR signal into two components – the symmetric signal (R_{xy}^s and R_{xx}^s) of a pure planar Hall response and the anti-symmetric signal (R_{xy}^a and R_{xx}^a) arising from an anomalous PHE contribution. Fig. 2 shows R_{xy}^s , R_{xy}^a and R_{xx}^s versus B plotted for the $\varphi = 0$ [fig. 2(g), (h) and (i)] and $\varphi = 90^\circ$ [fig. 2 (j), (k) (l)] configuration at $T = 1.6$ K. The R_{xy}^s and R_{xx}^s show the

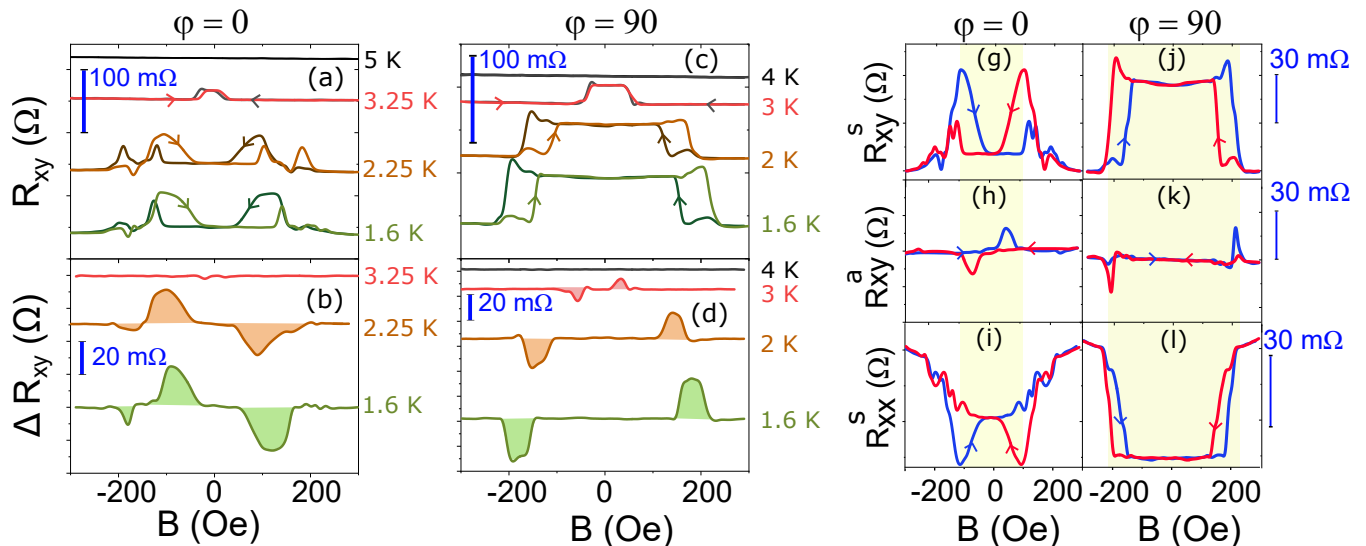


FIG. 2. (a), (c) Transverse resistance R_{xy} versus in-plane magnetic field B at different temperatures. (b), (d) The difference curves of forward and backward moving curves, representing hysteresis. (g), (j) Symmetric component of R_{xy} , R_{xy}^s vs B ; (h), (k) the anti-symmetric component R_{xy}^a vs B ; (i), (j) the symmetric component R_{xx} vs B , all at $T = 1.6$ K. Measurement configurations of the curves ($\varphi = 0^\circ$, $\varphi = 90^\circ$), are as mentioned on top. Scan direction of magnetic field is shown by arrows on the curves. $R_{xy}^s = \frac{R_{xy}^{+B} + R_{xy}^{-B}}{2}$, $R_{xy}^a = \frac{R_{xy}^{+B} - R_{xy}^{-B}}{2}$, $R_{xx}^s = \frac{R_{xx}^{+B} + R_{xx}^{-B}}{2}$.

expected inverted behavior with a similar range of variation: ≈ 65 m Ω . For simplicity, in the following discussions we focus our analysis only on the forward scan data. Similar arguments can be extended to the backward scan plots. In the forward scan, R_{xy}^s (R_{xx}^s) exhibits a peak (drop) at $B \approx -150$ Oe (-200 Oe) in $\varphi = 0$ ($\varphi = 90^\circ$) configuration [fig 2 (g) and (j)], corresponding to the magnetic phase transition described in fig. 1. Subsequently, a region of plateauing is observed in R_{xy}^s and R_{xx}^s indicating the stability of a magnetic phase. For the case of $\varphi = 90^\circ$ configuration, this plateau region persist over a broader range of B (-140 Oe $\lesssim B \lesssim 200$ Oe). Within this region, a hump develops in R_{xy}^a vs B , peaking at ≈ -50 Oe (≈ 200 Oe) in $\varphi = 0$ ($\varphi = 90^\circ$) configuration [fig 2 (h) and (k)], which resembles topological Hall effect (THE) [10]. We have verified that this signal arises from the non-trivial spin-texture at the interface captured in the true planar Hall measurement and not due to an out-of-plane component of B caused by a misalignment in the measurement. Subsequent to the plateau region in R_{xy}^s and R_{xx}^s , the signals oscillate over a small region in $\varphi = 0$ configuration between ≈ 100 Oe and 200 Oe after which the applied field aligns the interfacial spins along its direction. In contrast, the $\varphi = 90^\circ$ configuration shows an abrupt transition at 200 Oe. Very similar transitions but without any hysteresis or in-plane anisotropy in φ was observed in $\text{Bi}_2\text{Se}_3/\text{EuS}$ studies (see SI), owing to unfavourable growth or interface conditions. We further probe the presence of hump-like feature in R_{xy}^a by rotating the field out-of-plane. Here R_{xy}^a vs B measured in $\theta = 30^\circ$ configuration show a weak hysteretic

behavior at $B \approx 180$ Oe resembling the THE signal (see SI). In this configuration, the hump appears at a similar value of B with respect to the PHE study, thereby ruling out the formation of a conventional out-of-plane skyrmion state. This is further supported by the disappearance of the hump-like feature in the out-of-plane $\theta = 90^\circ$ configuration (refer to SI), elucidating that the formation of non-trivial spin-textures preserves the in-plane magnetic anisotropy.

We now describe the complete φ -dependence ($0^\circ \leq \varphi \leq 90^\circ$) of PHE by plotting the surface maps of R_{xy}^s and R_{xx}^s in fig. 3, with varying B and φ . Figure 3 (a), (c) and figure 3 (b), (d) shows the data corresponding to forward and backward scans respectively, that appear as mirror images capturing all the critical features. Region I represents the magnetic field regime where collinear magnetization dominates, region II, III and IV represent the regime where non-collinear spin phases are stabilized. Interestingly, we find that the phase transitions of initial creation (region I \rightarrow region II) and final annihilation (region IV \rightarrow region I) of the interface spin-textures occur independent of φ . We also observe oscillations around the region A that persist only in the low φ regime. This response may imply spin fluctuations concomitant with the phase transition. Furthermore, the R_{xy}^a vs B curve reveals a THE-like hump within the plateau region (see SI), corroborating the presence of non-trivial spin states. This plateau region broadens with increasing φ , shown by the merger of region II and III, indicating an anisotropy in the electronic detection of the spin-textures.

It is worthwhile to remark that the conduction in the

device is a result of electronic states at the interface and the bulk electronic transport in the TI. A pure TI without EuS in proximity shows no unconventional transport (see SI), implying that the features observed here, are dominated solely from the spin textures at the interface. The observed anisotropy in the electronic detection can arise due to two possible scenarios. First, where the spin-texture has a planar asymmetry; here, the additional Berry phase acquired by the conduction electrons will depend on φ and contribute to the anisotropy in the R_{xy}^s and R_{xx}^s signal. Second, assuming a symmetric spin texture, the anisotropy may be attributed to deformation of the Fermi surface due to Zeeman effect on the Rashba states of the TI [34]. However, this is unlikely owing to multiple crystal domain state of the films; even films that lack hexagonal symmetry of Bi_2Te_3 (verified by reflective high energy electron diffraction) demonstrate this anisotropy. Additionally, the spin-momentum locking property of the Dirac surface states of the TI is absent in our devices by design, since the Fermi level is tuned ≈ 0.35 eV (carrier density $\approx 10^{20}$ cm^{-3}) deep into the conduction band from its edge.

The presence of underlying planar asymmetry in the spin-textures is unveiled in the low-field measurement range within the plateau region (region III). This is shown in fig. 3 (e)-(f) via a vertical line-cut in fig. 3 (a), (b), (c) and (d) surface maps at $B = 0$. Interestingly, a spontaneous signal of PHR and PMR is observed that deviates from the conventional φ -dependence of the PHE signal. We observe the PHR and PMR signal to be symmetric about $B = 0$ and $\varphi = \pi/2$, with a periodicity of π . Such a symmetry may be correlated to the symmetry of the real-space spin textures at the interface. This observed anomalous signal is symmetric about $B = 0$, as seen in fig. 3 (e), which is different from the proposed anomalous PHR in two dimensional systems [35–37]. Outside region III, there is no significant φ dependence of R_{xx} and R_{xy} , conventional PHE signal of Bi_2Te_3 is observed at high fields ($B \geq 1$ T - see SI) [28].

We remark that unlike the case of $\text{Bi}_2\text{Se}_3/\text{BaFeO}$ [10] having a PMA MI, spin textures in our devices are observed only in the planar configuration. Theoretically, formation of skyrmions in a PMA material cannot simultaneously support textures of opposite topological charge [23]. Hence, the PMA ensures the observation of THE at $\theta = 90^\circ$ configuration associated to a specific sign of topological charge. In contrast, spin-textures in the in-plane anisotropy materials are observed to be different as they can simultaneously support textures of opposite topological charge. As a result, the net compensating spin textures become inaccessible in the out-of-plane measurement configuration ($\theta = 90^\circ$). It is likely that the interface of $\text{Bi}_2\text{Te}_3/\text{EuS}$ support the formation of such in-plane spin textures that show the $\pi/2$ symmetry in φ [23]. We however cannot rule out the possibility of other such spin-textures such as conical spirals or

skyrmion tubes that are also proposed to give rise to planar THE [11, 38]. Overcoming the challenge of imaging such interfacial spin-textures in the future may provide a means to decipher the precise nature of the spin textures., opening the path for further detailed experiment via spectroscopic techniques.

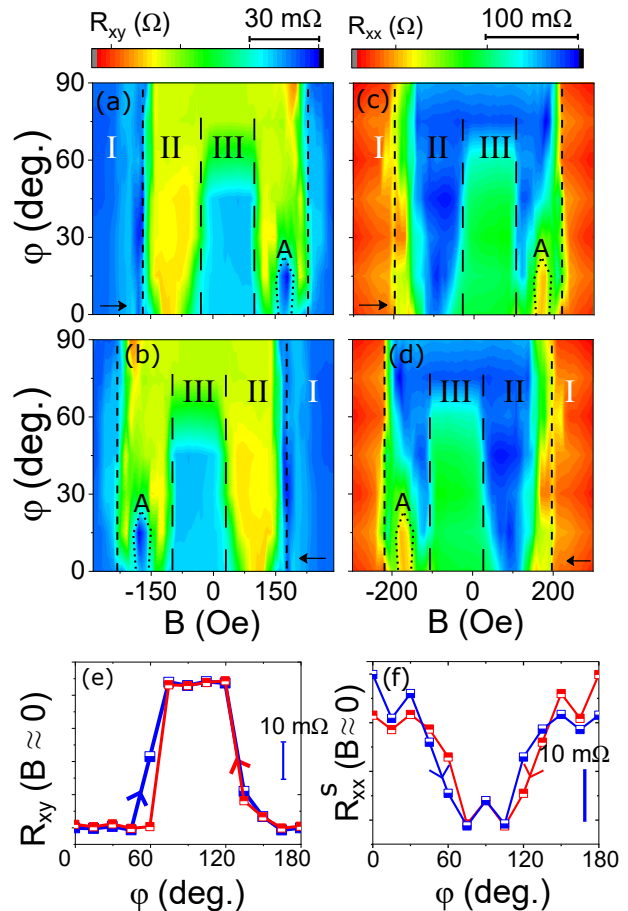


FIG. 3. Surface plots of symmetric components of R_{xy}^s vs B (a) forward scan direction (b) backward scan direction. Surface plots of symmetric components of R_{xx}^s (c) forward scan direction (d) backward scan direction. Data is symmetric about $\varphi = \pi/2$ (refer to SI for data of the full range $\varphi = 0^\circ$ to 180°). (e) R_{xy}^s at $B = 0$ and (f) R_{xx}^s at $B = 0$ extracted from the surface plot, as a function of φ .

To summarize, we have investigated the inverse proximity effect in a TI/MI system and reported the emergence of non-trivial spin textures in the planar Hall configuration. We find that these spin texture exhibit a spontaneous planar Hall signal symmetric about $\varphi = \pi/2$, providing experimental evidence of unconventional magnetic correlations responsible for emergent non-trivial in-plane spin textures in the interfacial EuS. Absence of anomalous Hall and topological Hall effect in the out-of-plane magnetic field configuration, corroborates our understanding that the correlations are dominated by in-plane anisotropy and reveal the extreme sensitivity of

the planar Hall measurement in detecting such unconventional spin-textures. This work therefore calls for further experimental and theoretical investigations in probing interfacial spin textures.

* dhavala.suri@gmail.com

† kvraman@tifrh.res.in

- [1] S. Mühlbauer, B. Binz, F. Jonietz, C. Pfleiderer, A. Rosch, A. Neubauer, R. Georgii, and P. Böni, *Science* **323**, 915 (2009).
- [2] N. Mathur, M. J. Stolt, and S. Jin, *APL Materials* **7**, 120703 (2019).
- [3] Q. Shao, Y. Liu, G. Yu, S. K. Kim, X. Che, C. Tang, Q. L. He, Y. Tserkovnyak, J. Shi, and K. L. Wang, *Nature Electronics* **2**, 182 (2019).
- [4] K. Yasuda, R. Wakatsuki, T. Morimoto, R. Yoshimi, A. Tsukazaki, K. S. Takahashi, M. Ezawa, M. Kawasaki, N. Nagaosa, and Y. Tokura, *Nature Physics* **12**, 555 (2016).
- [5] H. Wu, F. Groß, B. Dai, D. Lujan, S. A. Razavi, P. Zhang, Y. Liu, K. Sobotkiewich, J. Förster, M. Weigand, G. Schütz, X. Li, J. Gräfe, and K. L. Wang, *Advanced Materials* **32**, 2003380 (2020).
- [6] Q. L. He, G. Yin, L. Yu, A. J. Grutter, L. Pan, C.-Z. Chen, X. Che, G. Yu, B. Zhang, Q. Shao, A. L. Stern, B. Casas, J. Xia, X. Han, B. J. Kirby, R. K. Lake, K. T. Law, and K. L. Wang, *Phys. Rev. Lett.* **121**, 096802 (2018).
- [7] C. Liu, Y. Zang, W. Ruan, Y. Gong, K. He, X. Ma, Q.-K. Xue, and Y. Wang, *Phys. Rev. Lett.* **119**, 176809 (2017).
- [8] S. Zhang, F. Kronast, G. van der Laan, and T. Hesjedal, *Nano Letters* **18**, 1057 (2018).
- [9] J. Chen, L. Wang, M. Zhang, L. Zhou, R. Zhang, L. Jin, X. Wang, H. Qin, Y. Qiu, J. Mei, F. Ye, B. Xi, H. He, B. Li, and G. Wang, *Nano Letters* **19**, 6144 (2019).
- [10] P. Li, J. Ding, S. S.-L. Zhang, J. Kally, T. Pillsbury, O. G. Heinonen, G. Rimal, C. Bi, A. DeMann, S. B. Field, W. Wang, J. Tang, J. S. Jiang, A. Hoffmann, N. Samarth, and M. Wu, *Nano Letters* **21**, 84 (2021).
- [11] F. S. Nogueira, I. Eremin, F. Katmis, J. S. Moodera, J. van den Brink, and V. P. Kravchuk, *Phys. Rev. B* **98**, 060401 (2018).
- [12] X. Che, K. Murata, L. Pan, Q. L. He, G. Yu, Q. Shao, G. Yin, P. Deng, Y. Fan, B. Ma, X. Liang, B. Zhang, X. Han, L. Bi, Q.-H. Yang, H. Zhang, and K. L. Wang, *ACS Nano* **12**, 5042 (2018).
- [13] M. Lang, M. Montazeri, M. C. Onbasli, X. Kou, Y. Fan, P. Upadhyaya, K. Yao, F. Liu, Y. Jiang, W. Jiang, K. L. Wong, G. Yu, J. Tang, T. Nie, L. He, R. N. Schwartz, Y. Wang, C. A. Ross, and K. L. Wang, *Nano Letters* **14**, 3459 (2014).
- [14] C. Tang, C.-Z. Chang, G. Zhao, Y. Liu, Z. Jiang, C.-X. Liu, M. R. McCartney, D. J. Smith, T. Chen, J. S. Moodera, and J. Shi, *Science Advances* **3** (2017).
- [15] Y. T. Fanchiang, K. H. M. Chen, C. C. Tseng, C. C. Chen, C. K. Cheng, S. R. Yang, C. N. Wu, S. F. Lee, M. Hong, and J. Kwo, *Nature Communications* **9**, 223 (2018).
- [16] D. Liang, J. P. DeGrave, M. J. Stolt, Y. Tokura, and S. Jin, *Nature Communications* **6**, 8217 (2015).
- [17] F. Katmis, V. Lauter, F. S. Nogueira, B. A. Assaf, M. E. Jamer, P. Wei, B. Satpati, J. W. Freeland, I. Eremin, D. Heiman, P. Jarillo-Herrero, and J. S. Moodera, *Nature* **533**, 513 (2016).
- [18] P. Wei, F. Katmis, B. A. Assaf, H. Steinberg, P. Jarillo-Herrero, D. Heiman, and J. S. Moodera, *Phys. Rev. Lett.* **110**, 186807 (2013).
- [19] J. Kim, K.-W. Kim, H. Wang, J. Sinova, and R. Wu, *Phys. Rev. Lett.* **119**, 027201 (2017).
- [20] J. A. Krieger, Y. Ou, M. Caputo, A. Chikina, M. Döbeli, M.-A. Husanu, I. Keren, T. Prokscha, A. Suter, C.-Z. Chang, J. S. Moodera, V. N. Strocov, and Z. Salman, *Phys. Rev. B* **99**, 064423 (2019).
- [21] P. Wei, S. Lee, F. Lemaitre, L. Pinel, D. Cutaia, W. Cha, F. Katmis, Y. Zhu, D. Heiman, J. Hone, J. S. Moodera, and C.-T. Chen, *Nature Materials* **15**, 711 (2016).
- [22] S. Mathimalar, S. Sasmal, A. Bhardwaj, S. Abhaya, R. Pothala, S. Chaudhary, B. Satpati, and K. V. Raman, *npj Quantum Materials* **5**, 64 (2020).
- [23] K.-W. Moon, J. Yoon, C. Kim, and C. Hwang, *Phys. Rev. Applied* **12**, 064054 (2019).
- [24] M. Li, Q. Song, W. Zhao, J. A. Garlow, T.-H. Liu, L. Wu, Y. Zhu, J. S. Moodera, M. H. W. Chan, G. Chen, and C.-Z. Chang, *Phys. Rev. B* **96**, 201301 (2017).
- [25] H. Du, J. P. DeGrave, F. Xue, D. Liang, W. Ning, J. Yang, M. Tian, Y. Zhang, and S. Jin, *Nano Letters* **14**, 2026 (2014).
- [26] D. Rakhmievich, F. Wang, W. Zhao, M. H. W. Chan, J. S. Moodera, C. Liu, and C.-Z. Chang, *Phys. Rev. B* **98**, 094404 (2018).
- [27] A. A. Taskin, H. F. Legg, F. Yang, S. Sasaki, Y. Kanai, K. Matsumoto, A. Rosch, and Y. Ando, *Nature Communications* **8**, 1340 (2017).
- [28] A. Bhardwaj, S. Prasad P., K. V. Raman, and D. Suri, *Applied Physics Letters* **118**, 241901 (2021).
- [29] T. Yokouchi, N. Kanazawa, A. Tsukazaki, Y. Kozuka, A. Kikkawa, Y. Taguchi, M. Kawasaki, M. Ichikawa, F. Kagawa, and Y. Tokura, *Journal of the Physical Society of Japan* **84**, 104708 (2015).
- [30] N. Mathur, F. S. Yasin, M. J. Stolt, T. Nagai, K. Kimoto, H. Du, M. Tian, Y. Tokura, X. Yu, and S. Jin, *Advanced Functional Materials* **31**, 2008521 (2021).
- [31] T. Yokouchi, S. Hoshino, N. Kanazawa, A. Kikkawa, D. Morikawa, K. Shibata, T.-h. Arima, Y. Taguchi, F. Kagawa, N. Nagaosa, and Y. Tokura, *Science Advances* **4** (2018), 10.1126/sciadv.aat1115.
- [32] R. Ritz, M. Halder, C. Franz, A. Bauer, M. Wagner, R. Bamler, A. Rosch, and C. Pfleiderer, *Phys. Rev. B* **87**, 134424 (2013).
- [33] J. Liu, S. Zuo, H. Li, Y. Liu, X. Zheng, Y. Zhang, T. Zhao, F. Hu, J. Sun, and B. Shen, *Scripta Materialia* **187**, 268 (2020).
- [34] A. Soumyanarayanan, N. Reyren, A. Fert, and C. Panagopoulos, *Nature* **539**, 509 (2016).
- [35] R. Battilomo, N. Scopigno, and C. Ortix, *Phys. Rev. Research* **3**, L012006 (2021).
- [36] S. Bera and S. S. Mandal, *Journal of Physics: Condensed Matter* (2021).
- [37] P. Ho, A. K. Tan, S. Goolaup, A. G. Oyarce, M. Raju, L. Huang, A. Soumyanarayanan, and C. Panagopoulos, *Phys. Rev. Applied* **11**, 024064 (2019).
- [38] N. Mohanta, S. Okamoto, and E. Dagotto, *Phys. Rev. B* **102**, 064430 (2020).